Hindawi
Journal of Sensors
Volume 2017, Article ID 1308217, 11 pages
https://doi.org/10.1155/2017/1308217

Research Article

Fabrication of Si_3N_4-Based Artificial Basilar Membrane with ZnO Nanopillar Using MEMS Process

Jun-Hyuk Kwak,[1] Youngdo Jung,[2] Kyungjun Song,[2] and Shin Hur[2]

[1]*Center for Advanced Meta-Materials, Daejeon, Republic of Korea*
[2]*Department of Nature-Inspired Nanoconvergence System, Korea Institute of Machinery and Materials, Daejeon, Republic of Korea*

Correspondence should be addressed to Shin Hur; shur@kimm.re.kr

Received 19 February 2017; Accepted 31 May 2017; Published 9 July 2017

Academic Editor: Frederick Mailly

This paper presents the fabrication of Si_3N_4-based artificial basilar membrane (ABM) with ZnO nanopillar array. Structure of ABMs is composed of the logarithmically varying membrane fabricated by MEMS process and piezonanopillar array grown on the Si_3N_4-based membrane by hydrothermal method. We fabricate the bottom substrate containing Si_3N_4-based membrane for inducing the resonant motions from the sound wave and the top substrates of electrodes for acquiring electric signals. In addition, the bonding process of the top and bottom substrate is performed to build ABM device. Depending on sound wave input of the specific frequency, specific location of the ABM produces a resonant behavior. Then a local deformation of the piezonanopillar array produces an electric signal between top and bottom electrode. As experimental results of the fabricated ABM, the measured resonant frequencies are 2.34 kHz, 3.97 kHz, and 8.80 kHz and the produced electrical voltages on each resonant frequency are 794 nV, 398 nV, and 89 nV. Thus, this fabricated ABM device shows the possibility of being a biomimetic acoustic device.

1. Introduction

During the process of sound recognition in the human auditory system, the sound waves pass through the eardrums and ossicles (malleus, incus, and stapes) for sound amplification and then into the cochlea. Thereafter, the resonance-frequency separations occurred by the basilar membrane in the cochlea, and electric potentials are generated depending on the ion channels resulting from the delivered sound waves or the difference in sound pressures, which cause the amplitude of a section with the corresponding frequency of the sound waves to change [1–3]. The characteristics of the sound wave are then recognized by the auditory nerve. Basilar membranes extend from the inner ear base connected to the middle ear, all the way to the apex [4, 5]. The base is thick and narrow. Closer to the apex, it becomes thinner, wider, and less hard [6, 7]. Hence, a basilar membrane near the base demonstrates resonance to sound waves of high frequencies; closer to the apex, it demonstrates resonance to sound waves of low frequencies [7]. Since the resonant frequency varies depending on the position of the basilar membrane, this functions as a frequency analyzer [8, 9]. For biomimetic artificial basilar membrane (ABM), the frequency classification of basilar membranes depends on the principle of tonotopy [10–12]. Thus, the ABM covers all ranges of audible frequencies and induces local resonance in specific frequencies, at the same time. In the last 10 years, Professor Karl Grosh's group at the University of Michigan in 2005 produced a SiNx-type artificial basement membrane [13]. In 2011, Professor Ito's group at Tohoku University reported a study using a 40 μm thick piezoelectric film [10]. In addition, a research paper on ABM experiment using piezoelectric cantilever was presented by Professor Hongsoo Choi's group at DGIST in Korea in 2015 [12]. However, there has been no report on the development of artificial cochlear having continuous membrane capable of sound signal transmission in the similar fashion to that of human hair cell on the basilar membrane (BM). While artificial cochlear using cantilevers showed excellent frequency responses at its resonant frequencies, its structures differ from real human cochlear and can distinguish only discrete frequencies. In this paper, we present a continuous type (unlike cantilever type) SiNx artificial

basilar membrane on which ZnO nanowires are grown which mimic the real structure of a basilar membrane and hair cells in the human cochlear. It is proved that ZnO nanopillars converted nanoscale mechanical energy into electrical energy by means of piezoelectric zinc oxide nanowire arrays [14]. The ZnO nanopillars mimic hair cells of human cochlear. The generated biosignal by deforming the hair cells is transmitted to brain through hearing nerve [15]. Here, we study the electricity properties of ZnO nanopillars by deformation of the ZnO nanopillars. ZnO nanopillars are selectively patterned on the ABM substrate. The external sound moves the SiN_x membrane, which deforms the nanopillars, generating electricity; the electric signal generated is passed to the upper electrode of the ABM. The film electrode is used for obtaining the vibration signal and the final process is fabricated using a wafer-bonding technique, and the top and bottom wafers are separated by a microelectromechanical system (MEMS) process.

2. Fabrication of ABM Device

2.1. Design of ABM Structure. We also know that the cantilever method is very simple method and shows excellent unique peaks. However, since the cantilever is an open structure, it cannot contain the liquid (perilymph) like the BM of the actual cochlea. In addition, when human hears sound, complex frequencies are input into the ear. In such a complex situation, distinguishing a unique frequency does not have advantages in order to mimic the cochlear. Generally, the human cochlea consists of a spiral tube that is coiled about two and one-half turns around a hollow central pillar, the modiolus. It forms a cone approximately 9 millimeters (0.35 inch) in diameter at its base and 5 millimeters in height. When stretched out, the tube is approximately 30 millimeters in length; it is width about 2 millimeters. In this study, an ABM structure has a logarithmically varying membrane. The length of ABM with 32 bottom electrodes is 40 mm and width of membrane varies from 80 μm to 600 μm. Each bottom electrode is connected to a wire bonding pad. A top electrode is used as a common electrode and is electrically connected to the upper part of the bottom substrate through an Sn/Au bonding pad and then to the wire bonding pad at the upper side of the bottom substrate, acting as the common ground. Figure 1 shows the design schematic of a Si_3N_4 ABM.

2.2. Fabrication Process of ABM Structure. A piezonanopillar ABM contains low-stress SiN*x* vibration membranes. The piezonanopillar ABM fabrication process consists mainly of the fabrication of the top substrate for electric signal acquisition and the fabrication of the bottom ABM substrate for realizing the mechanical resonant motions and electrical signal generations. The fabrication of the bottom ABM substrate is divided into the fabrication of the vibration membranes that respond to the sound waves, the vibration membrane of the nanopillar array at the resonant frequency converts mechanical deformation to electrical generation, and the deposition of a bonding layer on the top electrode layer for the transport of electric signals. Figure 2 shows a general outline of ABM fabrication process.

2.2.1. Fabrication of Bottom Substrate of ABM Structure

(1) MEMS Process of Bottom ABM Substrate. Low-stress SiN*x* was used because the sound signal inputs to an ABM cause resonance at certain locations in vibrating membrane. For etching the bottom of the ABM substrate, a double side polished (DSP) Si wafer was utilized. The prepared DSP Si wafer was placed in a furnace and 2 μm of thermal oxide was grown all over the wafer. Silicon nitride of 0.3 μm was deposited on the bottom substrate on which the thermal oxide was formed through low pressure chemical vapor deposition (LPCVD) process. Silicon nitride was patterned through a photolithography process and then selectively etched. And then, we coated Polyimide on ABM membrane for producing a section to be used as an electrode at the top of the bottom substrate; an evaporator was utilized for Au (500 nm)/Ti (25 nm) deposition. Patterning of the bottom electrodes by photolithography was followed by selective etching of Au/Ti. At the locations of the vibration membranes to be processed, seed-layer patterning was performed through the lift-off process and photolithography in order to grow ZnO piezonanopillars. Atomic layer deposition (ALD) was then utilized for the ZnO seed-layer deposition. As for the ZnO piezonanopillars, ZnO nanowires were grown by using a low-temperature growth method. To protect the grown ZnO piezonanopillars in the subsequent processes, photoresist (PR) passivation was performed on the upper part of the bottom substrate. The final process was etched the Si, to enable it to function as a vibration membrane. Deep reactive ion etching (RIE) was applied for the selective etching of Si using the patterned silicon oxide as a mask. The etching process stopped at the silicon oxide layer over the top of the bottom substrate. Buffered hydrofluoric (BHF) solution was then used to remove the silicon oxide layer at the bottom of the top substrate silicon nitride layer. The PRs, which functioned as protective films for the ZnO nanopillar, were removed using acetone, and then vibration membranes of the ABM were formed, the backsides of which were etched. Figure 3 shows the fabrication process of the bottom substrate and Figure 4 shows the fabricated wafer of the bottom ABM substrate.

(2) Growth of ZnO Nanopillar Array. As mentioned in Section 2.2.1(1), the ZnO nanopillar can be grown on substrates on which ZnO seed layers on SiN*x* have been deposited. As for the ZnO seed layers, in order to solve the problem of lattice mismatch between the polymer substrate and the ZnO nanopillar and in order that the nuclear generation of ZnO nanopillars homojunctions easily occurs, the deposition of the ZnO seed layer (50 nm) on a polymer by plasma-enhanced atomic layer deposition (PEALD) is followed by the ZnO nanopillar growing process at low temperatures (~90°C) for 2 h in 0.05 M zinc nitrate hexahydrate ($Zn(NO_3)_2{\cdot}6H_2O$) and hexamethylenetetramine (HMTA, $C_6H_{12}N_4$), each at a pH of 6.8, through hydrothermal synthesis (Figure 5).

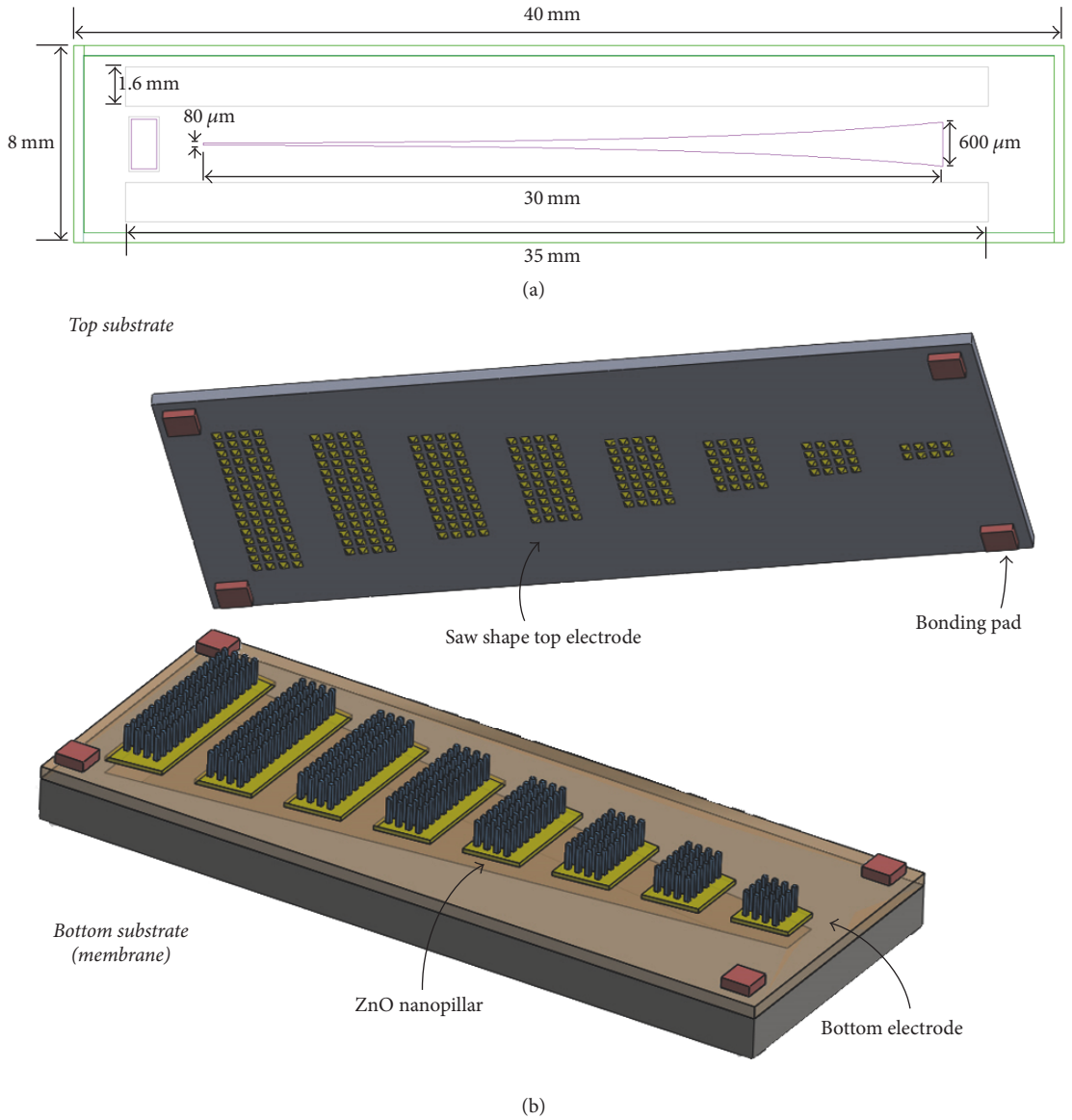

Figure 1: Design of Si_3N_4 ABM: (a) dimensions of Si_3N_4 ABM; (b) conceptual schematic of Si_3N_4 ABM.

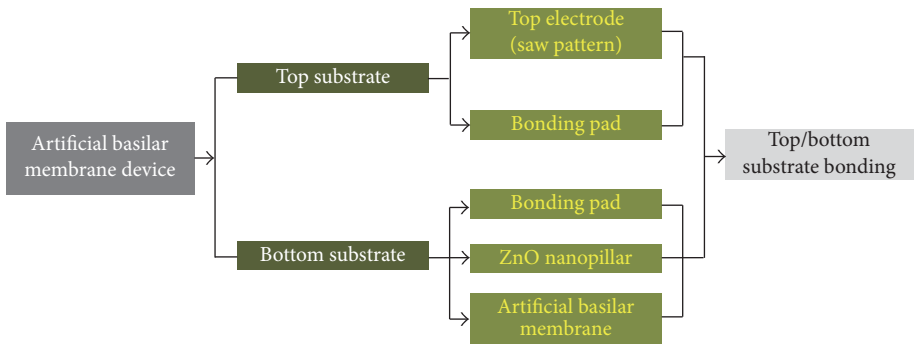

Figure 2: Flow chart of Si_3N_4 ABM fabrication process.

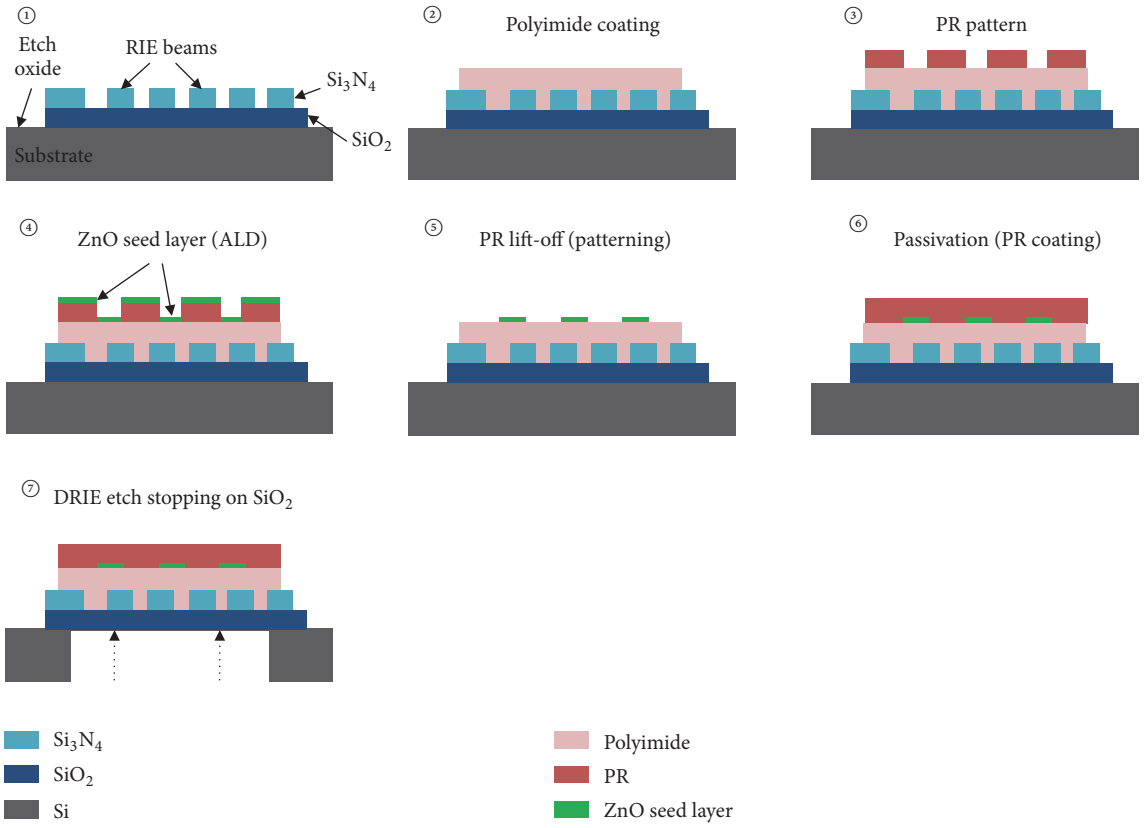

Figure 3: Fabrication process of bottom ABM substrate.

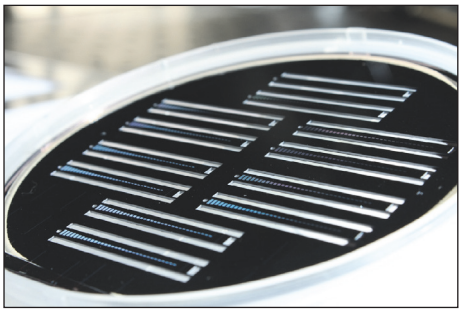

Figure 4: Fabricated wafer of bottom ABM substrate.

2.2.2. Fabrication of the Top Electrode. To measure the electric current generated by the piezoeffect in the ZnO nanopillar, the charge from the bent ZnO nanopillar is required. Since the location and shape of the electrode are important in this regard, saw-toothed electrodes were chosen to maximize the bending effect of the ZnO nanopillar. By treating the DSP silicon wafer in a furnace, 200 nm of SiO_2 was grown by the wet-oxidation process. PR patterning through the photolithography process was followed by SiO etching by means of buffered oxide etchant. Si etching was also conducted using 30% potassium hydroxide. The remaining SiO_2 was removed by means of BOE. Patterning through the photolithography process for lift-off was followed by SiO_2 deposition by plasma-enhanced chemical vapor deposition (PECVD). SiO_2 etching up to the corresponding thickness by means of BOE was followed by Au/Ti deposition utilizing an e-beam evaporator. Finally, saw-patterned electrodes were formed by etching Au/Ti after patterning by means of photolithography. Figure 6(a) shows the top electrode fabrication process. Figure 6(b) shows the SEM image of the fabricated top electrode with saw pattern.

2.2.3. Formation of Top/Bottom Electrode Bonding Layers. To deliver the electric signals by linking the top and bottom electrodes, Sn/Au eutectic bonding was implemented. The top electrodes connected to the top of the bottom substrate through Sn/Au eutectic bonding were connected between the Sn/Au bonding site in the bottom substrate and the

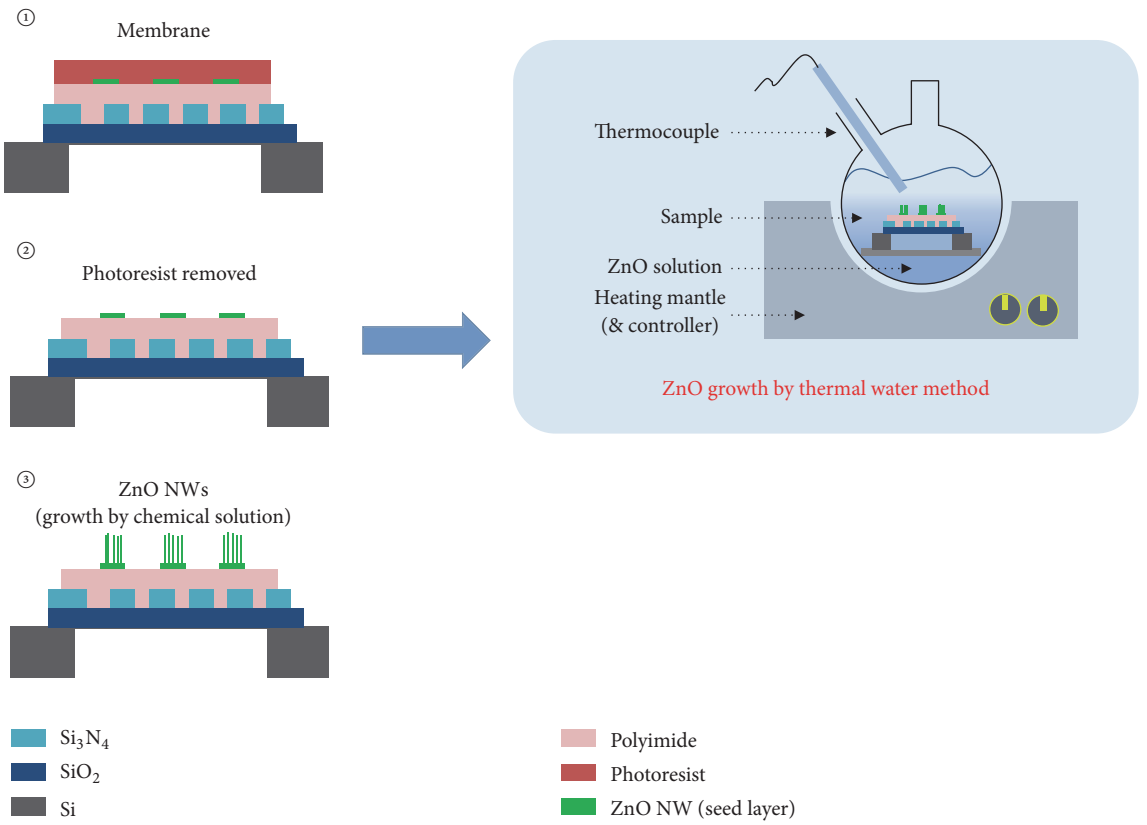

Figure 5: Growth of ZnO nanopillar on the bottom ABM substrate.

contact pad, for convenient signal processing. As for the Sn/Au eutectic bonding of the top and bottom substrates, the top electrode is connected to the top of the bottom substrate, while each corner of the bottom of the top substrate is connected to the corresponding section of the top of the bottom substrate. Figure 7 shows the electrode design applicable to the top/bottom substrates and an image of the completed Si_3N_4 ABM.

3. Experimental Results and Discussion

3.1. Mechanical and Electrical Characteristics of ZnO Nanopillar Array. The structure of the ZnO nanopillar array grown on a vibration membrane was analyzed using scanning electron microscopy (SEM) and current atomic force microscopy (I-AFM). The electrical characteristics were examined using an I-AFM module. The I-AFM measurement without the top electrode is purposed to verify the generation of electricity in the ZnO nanowire. When the ZnO nanopillar was pushed down using the AFM tip, electric signals were obtained in the controller through the electrodes connected to the AFM tip. Figure 8 shows the basic measurement diagram: electric signals from the ZnO nanopillar are obtained by means of I-AFM. The Park System XE-100 model was utilized as the AFM equipment. Figures 8(a) and 8(b) show the measurement method of I-AFM and the image of I-AFM, respectively.

The SEM images show ZnO nanopillars grown vertically on the vibration membrane. As shown in the SEM image in Figure 9, the ZnO nanopillars were combined with the vibration membranes and formed vertically.

The contact mode of AFM was utilized for the I-AFM-based current measurement. The scan size was 45 μm × 45 μm (sample size was 15 μm × 15 μm), the scan rate was 1 Hz, and the set point (force applied to the tip) was 300 nN. Figure 10 shows the current image of the ZnO nanopillars analyzed by I-AFM. It also shows the current values of the ZnO nanopillars measured by I-AFM. The maximum current value was 6.25 nA, and the average of three measurements was 3.5 nA.

3.2. Measurement of Mechanical and Electrical Properties of ABM Device. The final fabrication process in the ABM structure is the bonding process: the electrode of top substrate and the ZnO nanopillar array of bottom ABM substrate are combined in this process, in which it is quite difficult to implement an eutectic bonding due to many variables. To verify the thickness of bonding on the fabricated ABM, part of the element was solidified using an epoxy resin. The bonding part was then separated, and the surface was polished using fine sand paper. This sample was analyzed through SEM analysis. Figure 11 shows the SEM analysis process. The gap in the bonding was about 6 μm, a bit wider than the expected value of 5.5 μm. This is enough for the electric signal acquisition from the contact between the top electrode and the backside of the ZnO nanopillar array.

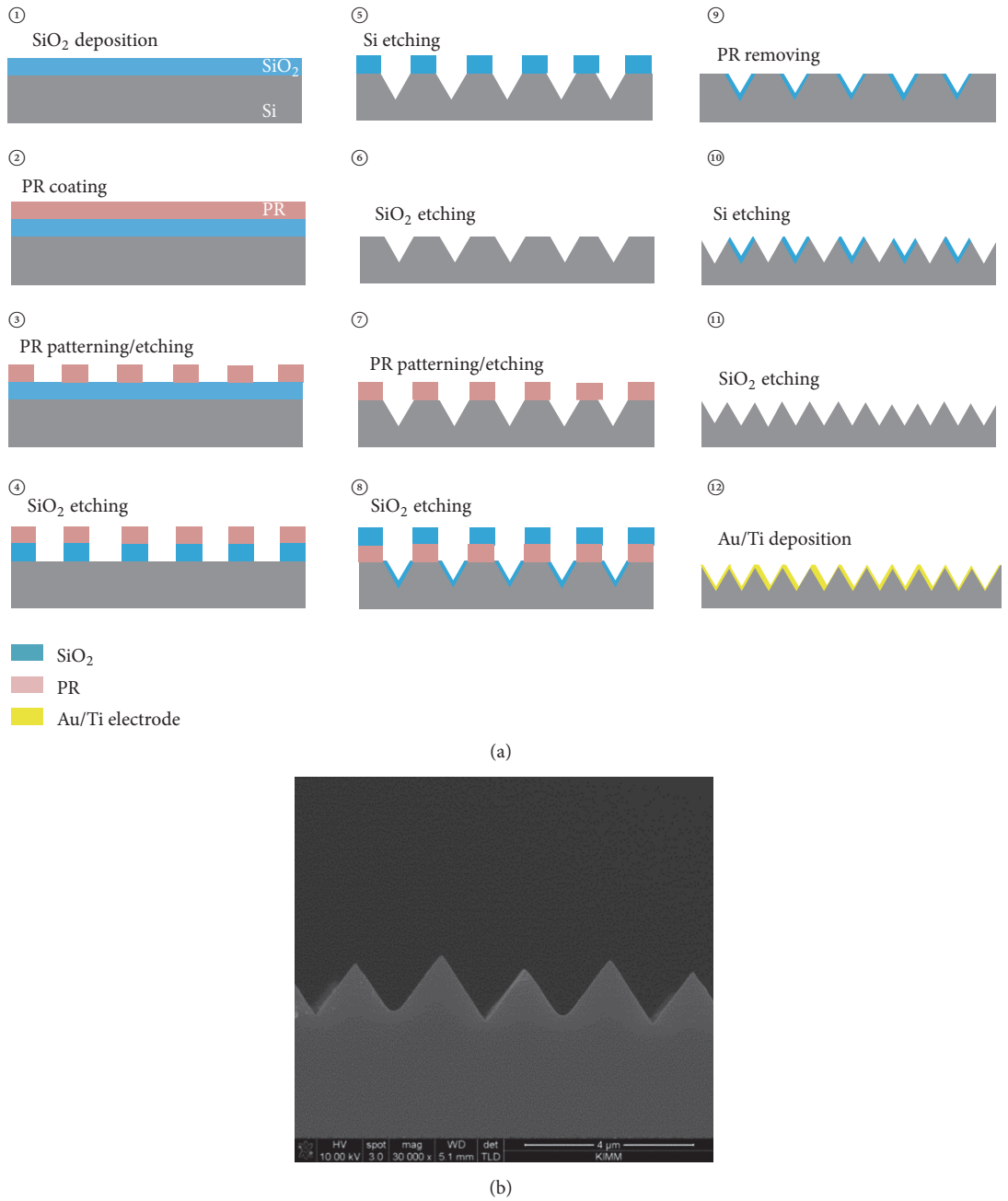

Figure 6: Fabrication of top electrode substrate: (a) fabrication process of top electrode with saw pattern; (b) SEM image of saw-patterned electrode.

In addition, an electrical measuring device for the nanopillar-type ABM was designed to measure the electrical signal generated by sound input. The laser Doppler vibrometer (PSV-I-400, Polytec, Germany) is an optical transducer used for determining displacement from membrane sample. The entire system was set up on *a vibration* isolator for low frequency. The laser source is transmitted to the vibrating membrane by the sound source and the velocity change of the membrane is measured by laser Doppler vibrometer. The electrical signal is obtained by using a data acquisition device (NI 4497, National Instruments, USA) to acquire electrical signals from the vibrating membrane. A sensitivity (dB/Pa or v/Pa) was measured with a standard microphone before measuring the electrical signal. Based on this, the sensitivity of the data obtained from the membrane was calculated and expressed as dB SPL. Figure 12 shows the diagram and setup for electric signal measurement.

As mentioned, the ABM described in this paper has a very complex structure because it has a microgap between the upper saw electrode of top substrate and the nanopillar array

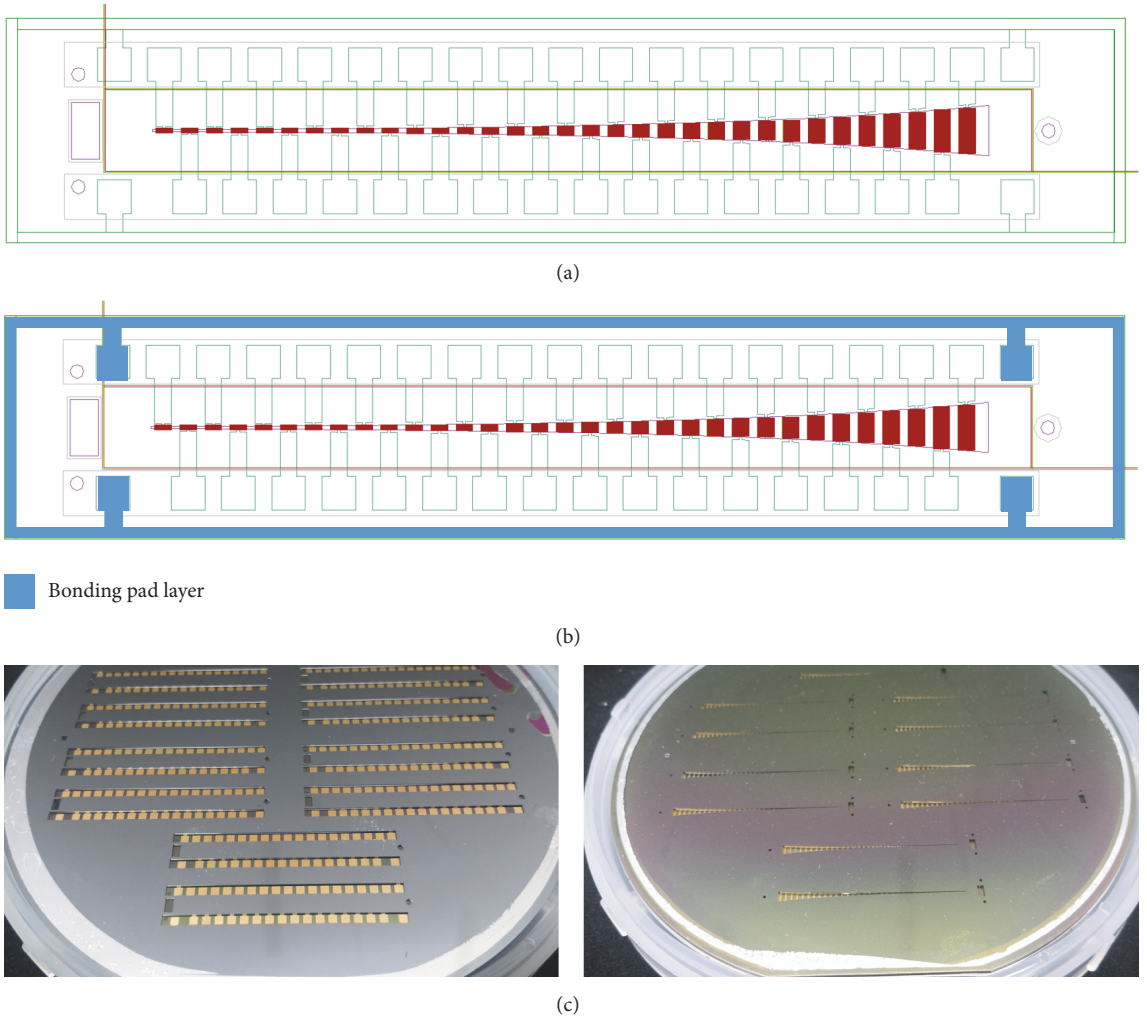

FIGURE 7: Layout of bonding pad: (a) unmarked bonding pad with ABM pattern; (b) narked (blue color) bonding pad with ABM pattern; and (c) images of the Si_3N_4 ABM: left (top wafer) and right (bottom wafer).

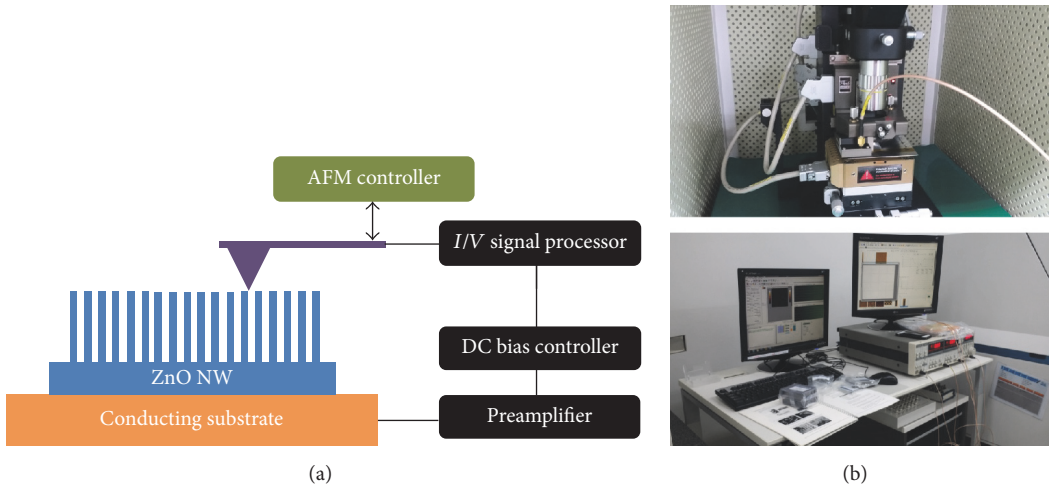

FIGURE 8: Electrical measurement setup for ZnO nanopillar: (a) measurement diagram for ZnO nanopillar array; (b) image of I-AFM setup.

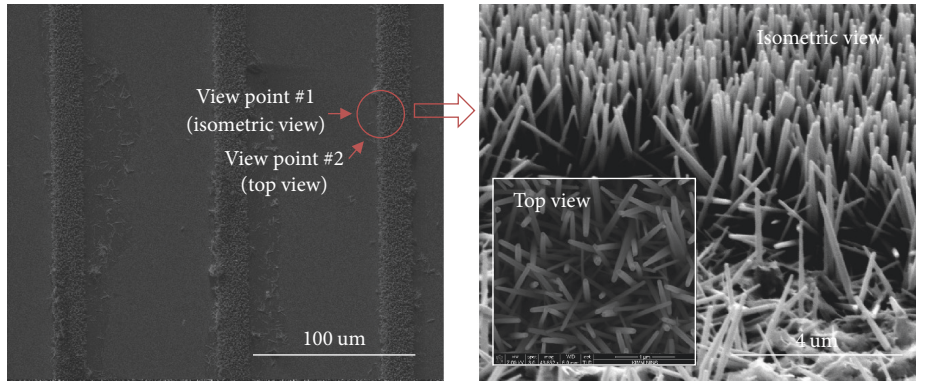

Figure 9: SEM image of ZnO nanopillar on the vibration membrane.

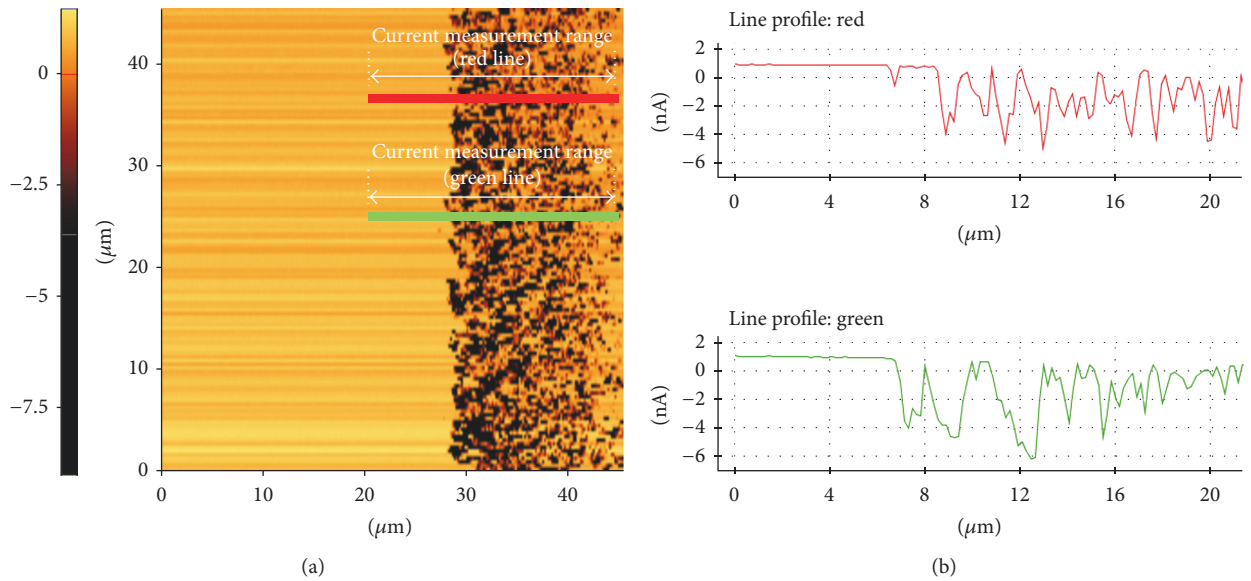

Figure 10: Measurement result of ZnO nanopillar array: (a) phase by current image; (b) electric measurement of ZnO nanopillar array.

of bottom ABM substrate. Therefore, it is difficult to obtain an electric signal from electrodes because ZnO nanopillar array has very small bending deformation. Nevertheless, electrical signals *were* measured from the three electrodes of the fabricated ABM device.

Figure 13 shows the measurement results of the mechanical and electric signals obtained from the fabricated ABM under frequency sweep conditions of 500 Hz to 10,000 Hz. Figure 13(a) shows the resonant displacements on vibrating membrane were measured with 13.4 nm, 2.9 nm, and 0.9 nm at sweep frequencies of 2.17 kHz, 4.10 kHz, and 9.15 kHz. Figure 13(b) shows the resonant electrical signals at electrode pad on ABM were measured with −122.7 dB (794 nV), −128.2 dB (398 nV), and −141.2 dB (89 nV) at sweep frequencies of 2.34 kHz, 3.97 kHz, and 8.80 kHz. The frequency differences between Figures 13(a) and 13(b) result from FFT processing of optical signal (laser Doppler vibrometer) and that of electrical signal, respectively. These differences may stem from the effect of phase shift due to the delay of the electrical signal acquisition. The time delay may come from a high-pass filter device in order to eliminate 60 Hz noise of electrical signal. Thus, an error about 5~10% may occur.

Also, as the height of ZnO nanopillar is not completely uniform, there are possibilities of contact noise. We can reduce this type of contact noise if the ZnO nanopillars are in contact with the saw electrodes constantly during their bending motion.

4. Conclusions

Biomimetic ABM structure with a logarithmically varying membrane was designed and fabricated by MEMS process and piezonanopillar array was grown on Si_3N_4-based membrane by hydrothermal method. Wafer bonding processes with top electrodes and bottom Si_3N_4-based membrane were performed for building ABM structures. The Sn/Au bonding pad was utilized as a channel for electric connection. Also, the piezo-ZnO-nanopillars electric property was measured by I-AFM test equipment and the maximum current measured during the bending was 3.84 nA. Test

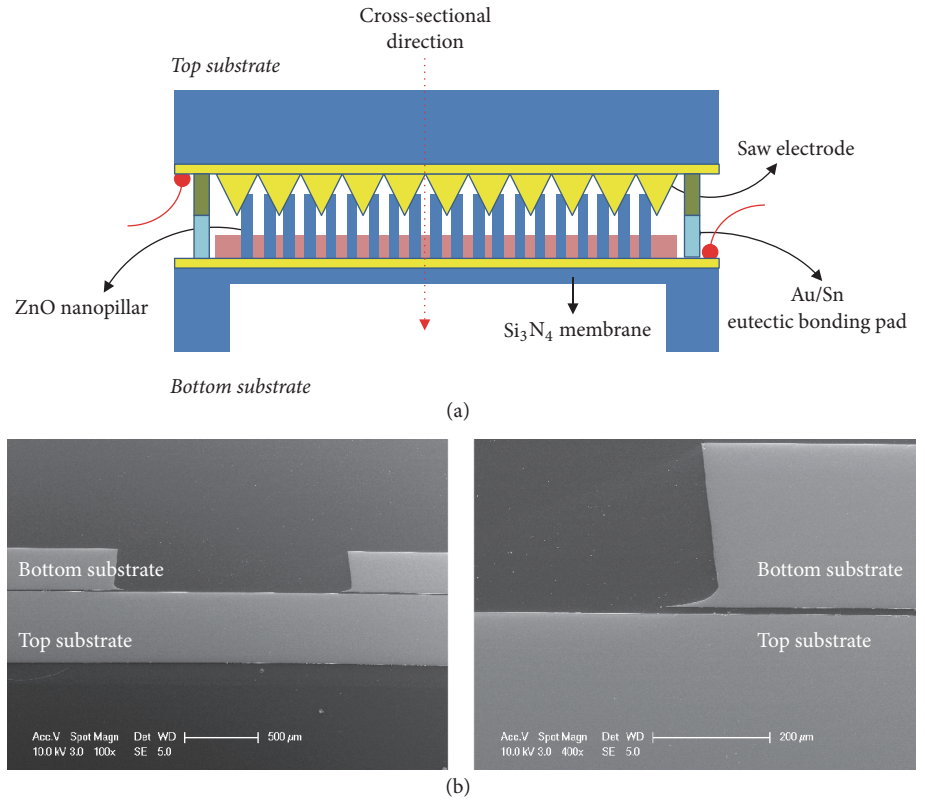

Figure 11: Analysis of bonding fabrication: (a) schematic of cross section of bonded ABM; (b) SEM image of bonding area by cross section.

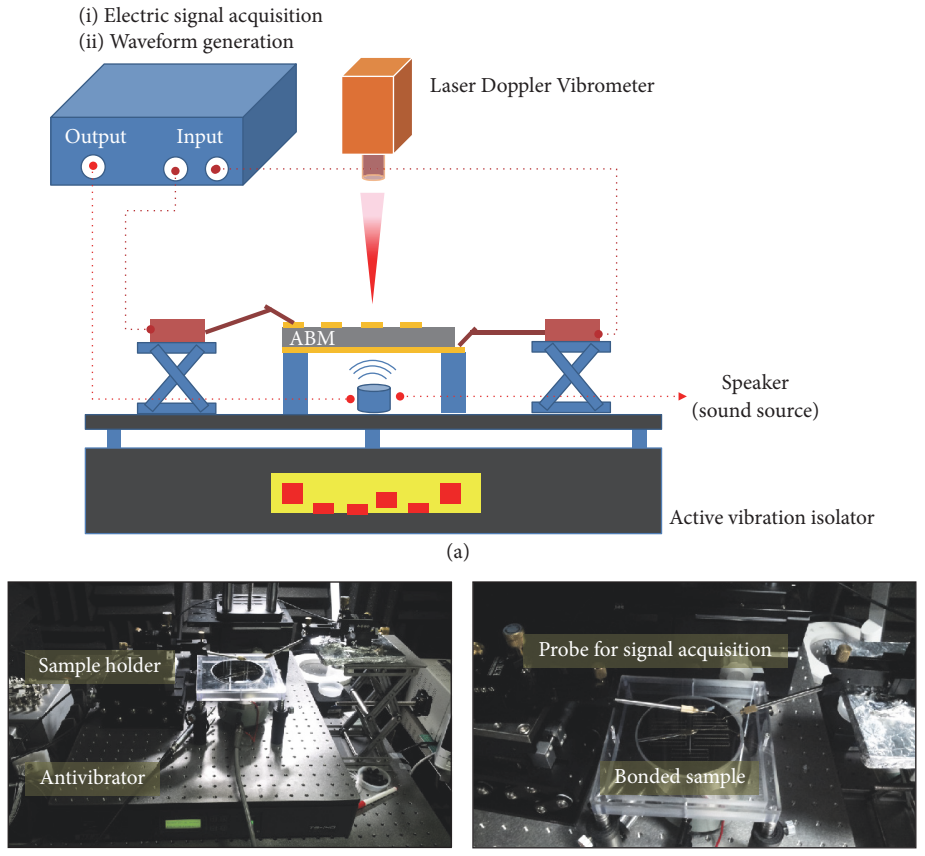

Figure 12: Measurement system for electric signal measurement: (a) schematic of system setup; (b) image of measurement part in anechoic room.

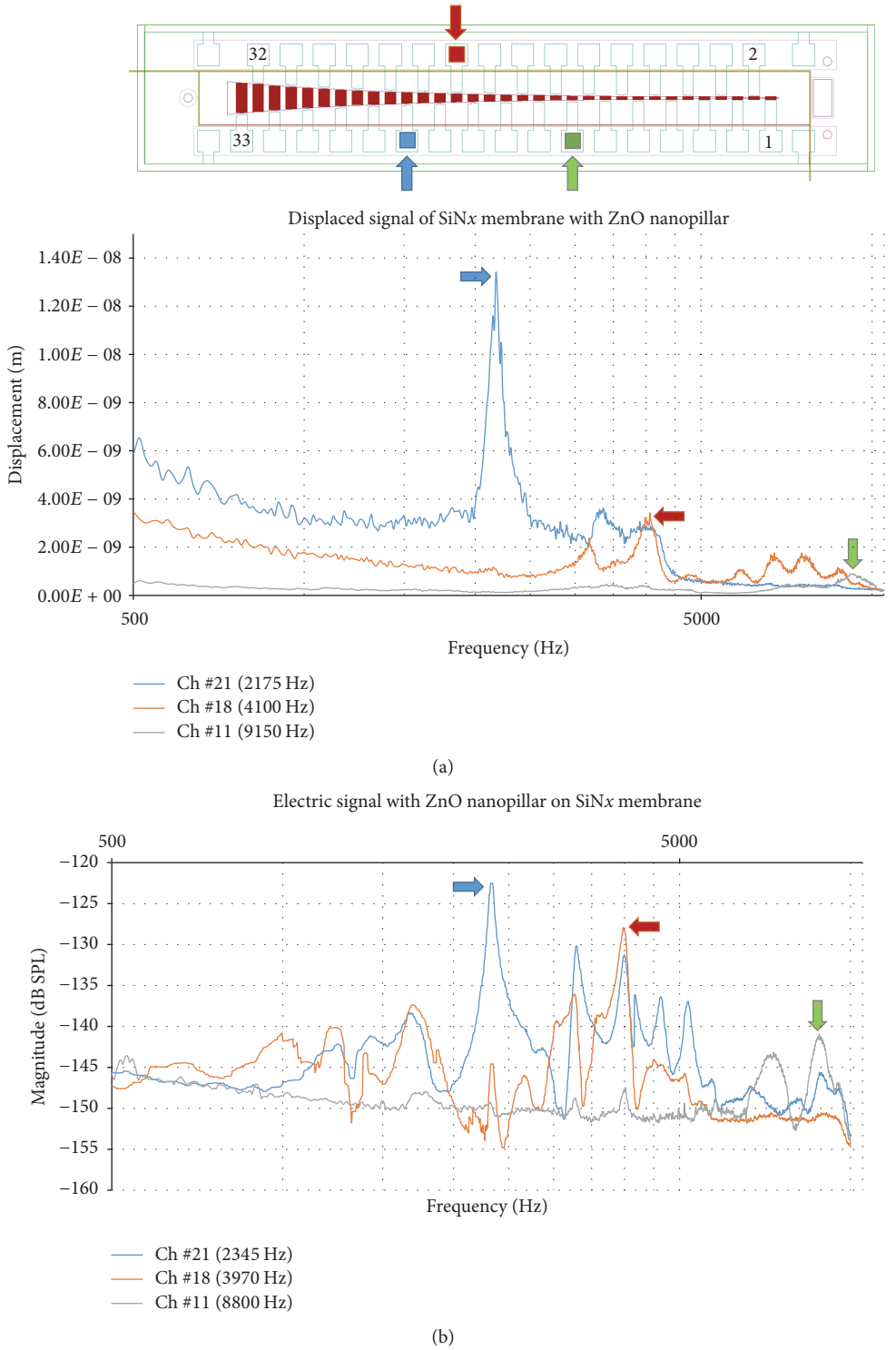

Figure 13: Mechanical and electrical test results of the fabricated ABM device: (a) test results of mechanical property; (b) test results of electrical property.

results of mechanical characteristics of the fabricated ABM show the resonant displacements 13.4 nm, 2.9 nm, and 0.9 nm at resonant frequencies of 2.17 kHz, 4.10 kHz, and 9.15 kHz. Test results of electrical characteristics show the resonant electrical amplitude −122.7 dB (794 nV), −128.2 dB (398 nV), and −141.2 dB (89 nV) at sweep frequencies of 2.34 kHz, 3.97 kHz, and 8.80 kHz. Also, because the height of ZnO nanopillar is not completely uniform, there are possibilities of contact noise. We can reduce this type of contact noise if the ZnO nanopillars are in contact with the saw electrodes constantly during their bending motion. Our ABM device shows a possibility as a biomimetic frequency analyzer that has the function of mechanical frequency separation and electrical signal generation on audible frequency range.

Conflicts of Interest

The authors declare no conflicts of interest.

Authors' Contributions

Jun-Hyuk Kwak, Youngdo Jung, and Kyungjun Song designed the artificial basilar membrane, performed experiments and analysis, and wrote the manuscript. Shin Hur analyzed mechanical properties of ZnO nanopillar and analyzed the experiments results.

Acknowledgments

This work was supported by the Center for Advanced Meta-Materials (CAMM), funded by the Ministry of Science, ICT, and Future Planning as a Global Frontier Project (NM8660), and Program of Creative technology (NK196E), funded by Korea Institute of Machinery and Materials (KIMM).

References

[1] D. T. Kemp, "Stimulated acoustic emissions from within the human auditory system," *The Journal of the Acoustical Society of America*, vol. 64, no. 5, pp. 1386–1391, 1978.

[2] G. von Békésy, "Some biophysical experiments from fifty years ago.," *Annual review of physiology*, vol. 36, pp. 1–16, 1974.

[3] D. T. Simon, S. Kurup, K. C. Larsson et al., "Organic electronics for precise delivery of neurotransmitters to modulate mammalian sensory function," *Nature Materials*, vol. 8, no. 9, pp. 742–746, 2009.

[4] F. Zeng, S. Rebscher, W. Harrison, X. Sun, and H. Feng, "Cochlear implants: system design, integration, and evaluation," *IEEE Reviews in Biomedical Engineering*, vol. 1, pp. 115–142, 2008.

[5] R. Z. Gan, B. P. Reeves, and X. Wang, "Modeling of sound transmission from ear canal to cochlea," *Annals of Biomedical Engineering*, vol. 35, no. 12, pp. 2180–2195, 2007.

[6] E. S. Olson, "Observing middle and inner ear mechanics with novel intracochlear pressure sensors," *The Journal of the Acoustical Society of America*, vol. 103, no. 6, pp. 3445–3463, 1998.

[7] J. P. Rauschecker and R. V. Shannon, "Sending sound to the brain," *Science*, vol. 295, no. 5557, pp. 1025–1029, 2002.

[8] R. Fettiplace and P. A. Fuchs, "Mechanisms of hair cell tuning," *Annual Review of Physiology*, vol. 61, pp. 809–834, 1999.

[9] R. Fettiplace, "Electrical tuning of hair cells in the inner ear," *Trends in Neurosciences*, vol. 10, no. 10, pp. 421–425, 1987.

[10] T. Inaoka, H. Shintaku, T. Nakagawa et al., "Piezoelectric materials mimic the function of the cochlear sensory epithelium," *Proceedings of the National Academy of Sciences of the United States of America*, vol. 108, no. 45, pp. 18390–18395, 2011.

[11] Y. Jung, J.-H. Kwak, Y. H. Lee, W. D. Kim, and S. Hur, "Development of a multi-channel piezoelectric acoustic sensor based on an artificial basilar membrane," *Sensors (Switzerland)*, vol. 14, no. 1, pp. 117–128, 2013.

[12] J. Jang, J. Lee, S. Woo et al., "A microelectromechanical system artificial basilar membrane based on a piezoelectric cantilever array and its characterization using an animal model," *Scientific Reports*, vol. 5, article 12447, 2015.

[13] R. D. White and K. Grosh, "Microengineered hydromechanical cochler model," *Proceedings of the National Academy of Sciences of the United States of America*, vol. 102, no. 5, pp. 1296–1301, 2005.

[14] Z. L. Wang and J. Song, "Piezoelectric nanogenerators based on zinc oxide nanowire arrays," *Science*, vol. 312, no. 5771, pp. 243–246, 2006.

[15] Y. Jung, J.-H. Kwak, H. Kang, W. Kim, and S. Hur, "Development of piezoelectric artificial cochlea inspired by human hearing organ," *Biomimetic and Biohybrid Systems*, vol. 9222, pp. 145–152, 2015.